The Role of Network Architecture in Collagen Mechanics

Karin A. Jansen,[1,2] Albert J. Licup,[3] Abhinav Sharma,[3,4] Robbie Rens,[3] Fred C. MacKintosh,[3,5,6,*] and Gijsje H. Koenderink[1,*]

[1]Biological Soft Matter Group, AMOLF, Amsterdam, the Netherlands; [2]Department of Pathology, University Medical Center Utrecht, Utrecht, the Netherlands; [3]Department of Physics and Astronomy, Vrije Universiteit, Amsterdam, the Netherlands; [4]Leibniz Institute for Polymer Research, Dresden, Germany; [5]Departments of Chemical & Biomolecular Engineering, Chemistry, and Physics & Astronomy, Rice University, Houston, Texas; and [6]Center for Theoretical Biophysics, Rice University, Houston, Texas

ABSTRACT Collagen forms fibrous networks that reinforce tissues and provide an extracellular matrix for cells. These networks exhibit remarkable strain-stiffening properties that tailor the mechanical functions of tissues and regulate cell behavior. Recent models explain this nonlinear behavior as an intrinsic feature of disordered networks of stiff fibers. Here, we experimentally validate this theoretical framework by measuring the elastic properties of collagen networks over a wide range of self-assembly conditions. We show that the model allows us to quantitatively relate both the linear and nonlinear elastic behavior of collagen networks to their underlying architecture. Specifically, we identify the local coordination number (or connectivity) $\langle z \rangle$ as a key architectural parameter that governs the elastic response of collagen. The network elastic response reveals that $\langle z \rangle$ decreases from 3.5 to 3 as the polymerization temperature is raised from 26 to 37°C while being weakly dependent on concentration. We furthermore infer a Young's modulus of 1.1 MPa for the collagen fibrils from the linear modulus. Scanning electron microscopy confirms that $\langle z \rangle$ is between three and four but is unable to detect the subtle changes in $\langle z \rangle$ with polymerization conditions that rheology is sensitive to. Finally, we show that, consistent with the model, the initial stress-stiffening response of collagen networks is controlled by the negative normal stress that builds up under shear. Our work provides a predictive framework to facilitate future studies of the regulatory effect of extracellular matrix molecules on collagen mechanics. Moreover, our findings can aid mechanobiological studies of wound healing, fibrosis, and cancer metastasis, which require collagen matrices with tunable mechanical properties.

INTRODUCTION

Collagens form a family of around 30 proteins that are crucial structural molecules in the human body (1). The most abundant family member is collagen type I, which forms fibrillar networks that shape and reinforce tissues such as skin, tendons, and bone. The structure of these networks is tailored toward diverse tissue-specific functions by auxiliary extracellular matrix molecules and by the biochemical and mechanical activities of cells. Collagen in load-bearing tendons, for instance, forms thick fibers (200 nm) that are aligned along the tendon to optimize force transmission and tendon strength (2). In contrast, collagen in the cornea forms woven sheets of thin fibers (~30 nm) that provide strength combined with optical transparency (3). Collagen in interstitial tissue forms mostly isotropic networks, which provide mechanical strength combined with porosity to facilitate nutrient transport and cell migration (4).

Collagen structure and mechanics not only determine the function of the tissue as a whole but also the functions of the cells that are resident in the tissue. Collagen fibers provide cells with topographical, biochemical, and mechanical cues, which regulate cell proliferation, differentiation, migration, and apoptosis (5). The mechanobiological interplay between cells and the surrounding collagen extracellular matrix is essential to guide physiological processes such as wound healing and immune cell trafficking, but it can also trigger pathological processes. Abnormal stiffening of interstitial collagen networks, for instance, promotes cell invasion, which contributes to cancer, atherosclerosis, and chronic fibrosis.

The importance of collagen mechanics in biology has triggered a long history of research on the relation between collagen structure and mechanics. It has long been known that collagenous tissues exhibit a distinctive nonlinear elasticity characterized by strain-induced stiffening (6). This

*Correspondence: fcmack@gmail.com or g.koenderink@amolf.nl

mechanical design allows tissues such as skin and arteries to be soft at low strain yet stiff at high strain, ensuring mechanical stability under large loads (7). However, the complex architecture of collagenous tissues, which comprises multiple scales, has made it difficult to pinpoint the structural basis of the strain-stiffening response. Tissues contain networks of fibril bundles, which in turn contain hundreds of molecules per cross section packed in an axially ordered lattice (8). In situ x-ray scattering studies suggest that multiple mechanisms operating at different length scales contribute to the overall mechanical response at the tissue level (9).

The challenge to elucidate the origin of the nonlinear elasticity of collagenous tissues has motivated intensive efforts to study simplified model systems reconstituted from purified collagen. This development was further fueled by the rapid growth of the interdisciplinary field of mechanobiology, in which reconstituted collagen networks are popular as tissue equivalents in basic studies of the biology of tissues, wound healing, immunity, and cancer and in more applied studies relating to regenerative medicine (10,11). Conveniently, the self-assembly of collagen into fibrillar networks is encoded in the collagen molecule itself. Under physiologically relevant buffer conditions, collagen spontaneously assembles into axially ordered fibrils, which branch and cross-link to form a three-dimensional (3D) network (1). The diameter of the fibrils can be tuned from tens of nanometers to several microns by changing environmental conditions such as the solution pH (12–14) and polymerization temperature (15–17).

It is well established that reconstituted collagen networks stiffen in a similar manner as whole tissues when they are subjected to a mechanical stretch or shear (12,18–21). However, even in this more simplified context of reconstituted networks, theoretical modeling remains challenging because of the range of scales. The most detailed models, based on full-atom simulations, are limited to single collagen molecules and microfibrils and require coarse-graining approaches to reach up to the fibril level (22,23). Recent models aimed to describe collagen at the network level therefore usually treat the fibrils as homogeneous elastic beams (20,24,25). These models predict that the elasticity of collagen networks is primarily governed by the local connectivity z, meaning the number of fibers that meet at each network junction. Because collagen fibers are connected by a combination of branch points ($z = 3$) and crosslinks ($z = 4$), z is on average between three and four (20,25,26). In networks of springs that possess only stretching energy, such a low connectivity is insufficient for mechanical stability in 3D, in which the isostatic limit is $z = 6$ (27). Fibrous networks such as collagen networks, however, are stabilized by the high bending rigidity of the fibers (20,28).

Recent experiments on reconstituted collagen I networks confirmed some of the predictions of these fiber-based network models (20,25,29). However, the general validity of this model for collagen networks reconstituted over a wider range of self-assembly conditions remains untested. Consequently, a clear consensus on the physical basis of the elasticity of collagen networks is still lacking. Random fiber models generally predict that the network stiffness at small strain should go up with collagen concentration as a power law with an exponent of two (30,31), but experimentally, a wide range of exponents between one and three has been observed (18,19,32–36). It was recently suggested that this range can be accounted for by a systematic variation in local architecture with concentration (25), although this hypothesis has yet to be tested experimentally. Moreover, this model also made another interesting prediction that still lacks experimental verification: strain-stiffening is predicted to be coupled to a build-up of a negative (contractile) normal stress under shear (20). Although there have been reports of negative normal stresses in filamentous networks including collagen (37,38), which is opposite to the response of most elastic solids and polymer hydrogels (37,39), the relationship of negative normal stress to strain-stiffening has not been quantitatively demonstrated experimentally.

The goal of this work is to quantitatively decipher the relation between the mechanics and underlying architecture of fibrillar collagen networks reconstituted from purified collagen I. We show that a model of disordered fiber networks provides a self-consistent framework to quantitatively explain both the linear and nonlinear elastic properties of collagen networks over a wide range of concentrations (0.5–5 mg/mL) and assembly temperatures (between 26 and 37°C). We probed the elastic properties of the networks by macroscopic shear rheometry and characterized the network architecture by combining light scattering, scanning electron microscopy, and confocal reflectance microscopy. We find that as the stress applied to a collagen network is increased, the network stiffens in two stages. In the first regime, network stiffening is coupled to the simultaneous build-up of self-generated negative normal stress, as predicted for bending-dominated networks (20). In the second stage, stiffening is caused by a mechanical phase transition to a stretch-dominated response above a critical strain value γ_c (25). Interestingly, our data suggest that the elastic properties of collagen networks are sensitive to subtle changes in network architecture with changing collagen concentration and polymerization temperature.

MATERIALS AND METHODS

A detailed description of the experimental and computational methods is provided in the online Supporting Materials and Methods. Experiments were performed on collagen networks reconstituted from rat-tail collagen type I in a buffer that is compatible with in vitro cell culture (Dulbecco's modified Eagle's medium cell culture, 1% fetal bovine serum, 50 mM HEPES, 1.5 mg/mL sodium bicarbonate, and 0.1% antibiotics (pH 7.3–7.4)). Networks were polymerized at temperatures between 22 and 37°C and at collagen concentrations between 0.7 and 5 mg/mL. Rheology was performed with a stress-controlled rheometer (Physica

MCR 501; Anton Paar, Graz, Austria) using a cone-plate geometry with 40-mm diameter and 1° cone angle. The networks were polymerized in situ for 6 h before rheological testing. Turbidity measurements were performed using a Cary300 UV-Vis spectrophotometer (Agilent Technologies, Amstelveen, the Netherlands) on networks prepared in plastic cuvettes (UV-Cuvette micro, Plastibrand, Germany) for 6 h or overnight. Rheological and turbidity data shown are averages ± SD for a minimum of three independently prepared samples. Collagen networks were imaged by confocal reflectance microscopy with an inverted Eclipse Ti microscope (Nikon, Tokyo, Japan), using a 488 Ar laser (Melles Griot, Albuquerque, NM) for illumination and a 100× numerical aperture 1.49 or 40× numerical aperture 1.30 objective. Fixed and dried networks of 4 mg/mL collagen coated with Au/Pd were imaged by scanning electron microscopy (Verios 460; FEI Company, Eindhoven, the Netherlands). Computational modeling of collagen networks was performed by representing the networks as two-dimensional (2D) disordered triangular lattices, described in detail elsewhere (20,25,40). These lattices have a spacing l_c and dimensions W × W, where $W = 50l_c$. We enforce local fourfold connectivity by a phantomization procedure, in which a binary cross-link is formed between two randomly selected fibers at each vertex while treating the third fiber as a phantom that does not interact with the other two fibers. Next, we reduce $\langle z \rangle$ to a value between three and four by bond dilution, which involves random removal of segments with a probability q. This procedure reduces the average fiber length to $L = l_c/q$. Thus, the networks are, by construction, subisostatic and floppy in the absence of bending interactions. Each filament is assigned a stretching modulus, μ_s, and a bending modulus, κ. The lattices are subjected to a simple shear strain, γ, and allowed to relax by minimization of the total elastic energy per unit volume, H, which is calculated according to a discrete form of the extensible wormlike chain Hamiltonian. The stress follows from the minimal energy as $\sigma = dH/d\gamma$, whereas the differential elastic shear modulus follows as $K = d^2H/d\gamma^2$. Stress and stiffness are measured in units of μ/l_c^{d-1}, where d is the dimensionality.

RESULTS

Collagen network architecture depends on polymerization conditions

Our goal was to quantitatively decipher the relation between the mechanics and underlying architecture of fibrillar collagen networks reconstituted from purified collagen I. To tune the structure of the networks, we varied the polymerization temperature, motivated by prior work demonstrating that temperature strongly influences the architecture of collagen networks (15,41,42). To visualize the network structure, we use confocal reflectance microscopy (CRM), which is an ideal technique for noninvasive and label-free imaging of collagen (43). We observe striking changes in network structure when we polymerize 4 mg/mL collagen at different temperatures between 22 and 37°C, as shown in the top row of images in Fig. 1 (see Fig. S1 for the full range of temperatures and a broader range of magnifications). The networks are dense, isotropic, and uniform

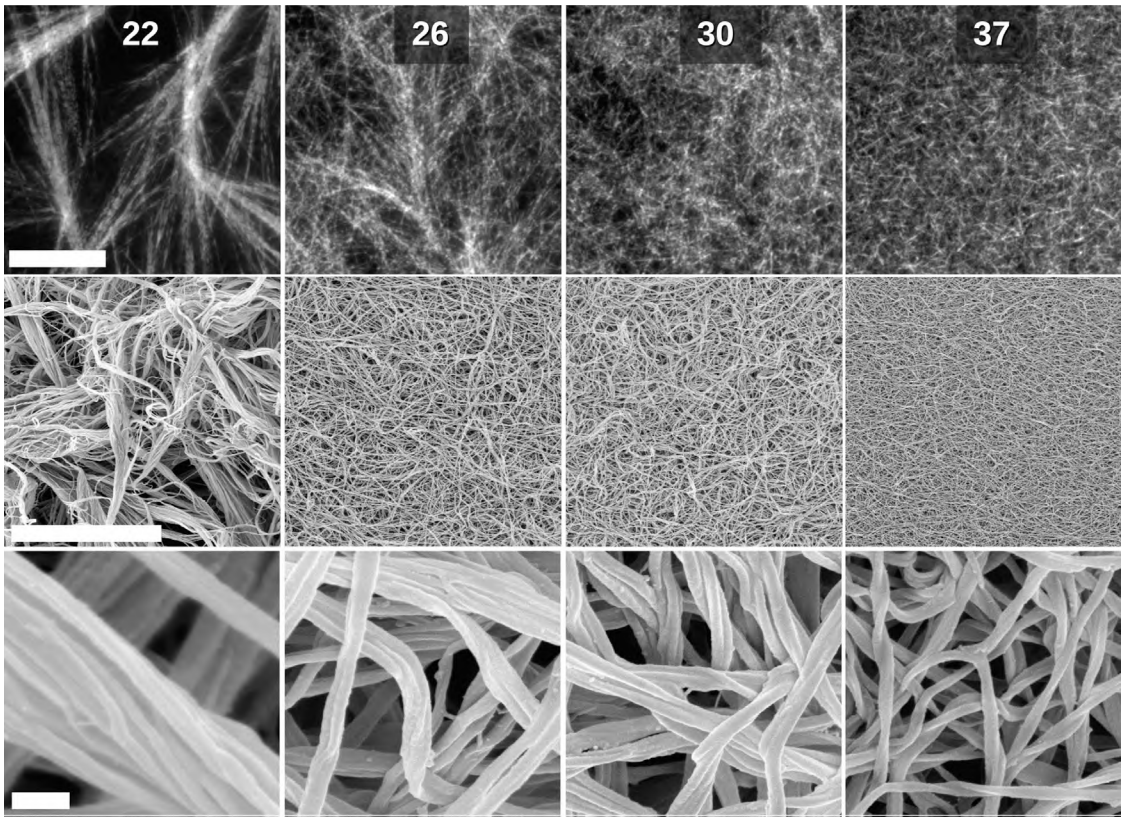

FIGURE 1 Temperature dependence of the microstructure of 4 mg/mL collagen networks. The temperature is indicated above each column in units of °C. Confocal reflection images (*row 1*), showing an open network of "fan-shaped" fibril bundles at 22°C and more homogeneous and progressively denser networks with increasing temperature, are given. SEM images are shown at two different magnifications (*rows 2* and *3*). The scale bars represent 20 μm (*rows 1* and *2*) and 200 nm (*row 3*). See Fig. S1 for additional data.

at temperatures of 30°C and above. In contrast, they appear more heterogeneous and open at lower temperatures, especially at 22°C, where we observe fan-shaped bundles of collagen fibrils. Similar fan-shaped bundles were observed previously at polymerization temperatures between 4 and 27°C (15,41,42) and were proposed to arise from the kinetic arrest of growing fibrils during network formation (42).

To obtain more high-resolution information regarding the network structure, we supplement confocal reflectance microscopy with scanning electron microscopy (SEM) of dehydrated networks. The fan-shaped bundles at 22°C are also visible in SEM images, in which they are seen to be bundles of fibrils that splay out at one end (Fig. 1, two *bottom rows*). Networks formed at 26°C also display bundles in SEM images, but their width is more uniform, and the network microstructure appears more uniform than at 22°C. As the temperature is raised further, the networks remain homogeneous and become progressively less bundled. At 37°C, the network looks homogeneous at all inspected length scales, and bundling is minimal. To quantify the change in diameter of the fibers (i.e., fibril bundles) with temperature, we measured the cross-sectional width of at least 250 randomly sampled fibers per condition in SEM images recorded at magnifications between 10,000 and 50,000 for three independently prepared samples. We did not attempt to perform this analysis for SEM images of networks prepared at 22°C because of the open fan shape of the collagen fibers of these networks. As shown in Fig. 2 *A*, the average fiber diameter is around 150 nm at temperatures of 26 and 30°C (with a large spread at 26°C), whereas it is around 70 nm at both 34 and 37°C. We note that these values are expected to be different from the actual diameters of the fibers in their native, hydrated state. On the one hand, fiber shrinkage is expected because of the solvent-removal procedure required to prepare samples for electron microscopy, whereas on the other hand, some thickening is expected because of the deposition of a metal coating that is required for imaging.

For comparison, we therefore also probed the fiber diameter by light scattering, a technique that is noninvasive and does not require dehydration (44). The basic idea is that the wavelength dependence of the turbidity of a fibrous gel, $\tau(\lambda)$, encodes information on the average diameter d and mass-length ratio μ of the fibers. Theoretical models for light scattering from random fiber networks (assumed to be monodisperse in diameter) predict that $\tau\lambda^5$ should increase linearly with λ^2 with a slope that depends on μ and an intercept dependent on μ and d (for details, see Supporting Materials and Methods). We indeed find approximately linear dependencies for collagen networks formed at temperatures between 26 and 37°C, consistent with the uniform microstructure seen in confocal reflectance microscopy and SEM images (Fig. S2). By contrast, we find a strongly nonlinear dependence for networks formed at 22°C, indicating that light scattering is sensitive to the structural

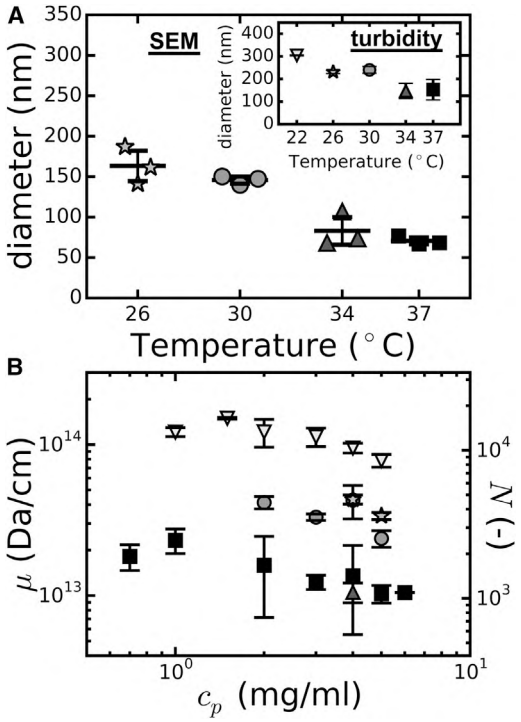

FIGURE 2 Comparison of fibril diameter measurements by electron microscopy on dried samples and turbidity measurements on hydrated samples. (*A*) Average fiber diameters for 4 mg/mL collagen networks polymerized at different temperatures, determined from SEM images (*main graph*) and turbidimetry (*inset*), are given. (*B*) The concentration dependence of the mass-length ratio obtained from turbidimetry for collagen networks formed at temperatures of 22° (*triangles down*), 26° (*stars*), 30 (*circles*), 34° (*triangles up*), and 37°C (*squares*) is given. The left *y* axis corresponds to the mass-length ratio μ, whereas the right *y* axis shows the corresponding number of monomers per fibril cross section, N (see Eq. S3). Turbidity data are averages ± SD for three samples per condition. SEM data are averages ± SD of three samples per condition, for which at least 250 fibrils were analyzed.

heterogeneities in these networks. The μ and d values obtained at 22°C (by fitting the data for wavelengths between 650 and 890 nm) should therefore be regarded as approximate.

The diameters obtained by light scattering are nearly twofold higher than the values obtained from SEM images, indicating that the dehydration procedure needed to prepare SEM samples induces fiber shrinkage (see Fig. 2 *A*). But the trend as a function of temperature is similar as observed by SEM: fibers formed at 22°C are thickest with an average diameter of 300 nm, fibers formed at 26 and 30°C have comparable average diameters of ~200 nm, and fibers formed at 34 and 37°C have smaller diameters of around 150 nm. The average mass-length ratio of the fibers also decreases with increasing polymerization temperature (see Fig. 2 *B*). From the change in μ, we can estimate the corresponding change in average mesh size, $\xi = (1/\rho_l)^{0.5}$, where $\rho_l = c_p/\mu$ is the total length of collagen fibers per unit volume (in m^{-2}) and c_p is the collagen concentration

(in mg/mL). At 4 mg/mL collagen, we expect a twofold reduction in ξ from 3.3 to 1.6 μm as the polymerization temperature is raised from 26 to 37°C, a trend that is qualitatively consistent with the confocal reflectance microscopy images. At each polymerization temperature, we find that both μ and d decrease with increasing collagen concentration (see Fig. 2 *B*; Fig. S2 *B*).

Collagen mechanics depend on polymerization conditions

Strain-stiffening behavior of collagen networks

To test how the changes in network structure identified by microscopy and turbidimetry influence collagen mechanics, we first investigated the nonlinear elastic response of the collagen networks. Specifically, we probed the differential modulus, $K' = \delta\sigma/\delta\gamma$, by subjecting the network to a stepwise increasing prestress, σ, while superposing small amplitude stress oscillations. We find that with increasing strain, the elastic modulus, K', strongly increases (Fig. 3 *A*) until a maximal strain of 20–50% is reached, at which the networks fail (Fig. S3). We will refer to this strain as the failure point, but we note that it is unclear whether failure is due to internal network rupture or detachment from the rheometer plates. The final stiffness just before network rupture is typically one order of magnitude higher than the linear modulus, consistent with prior reports (19,34). The strain-stiffening response is reversible for all networks formed between 26 and 37°C, with little hysteresis between forward and backward sweeps and reproducible strain-stiffening in consecutive runs (Fig. S4). By contrast, networks formed at 22°C show significant hysteresis and progressive softening in repeated stress ramps.

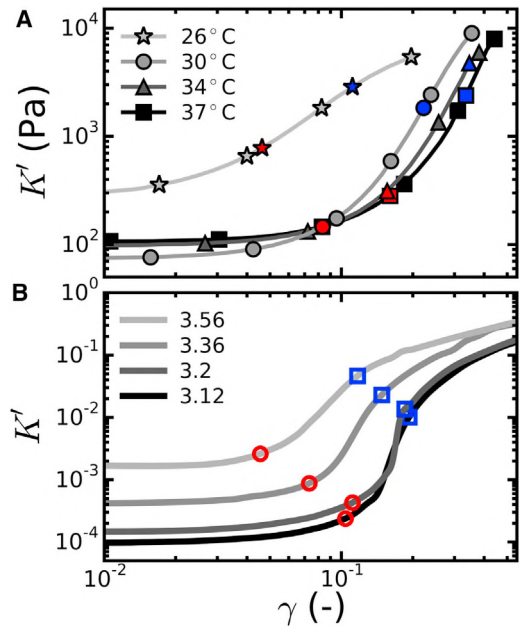

FIGURE 3 Comparison of the strain-stiffening response of collagen networks with simulations of disordered 2D fibrous networks. The differential elastic modulus K' is plotted as a function of the applied shear strain, γ. Red symbols denote the onset strain at which stiffening sets in (γ_0; see Fig. S5). Blue symbols denote the critical strain for the transition to stretch-dominated elasticity (γ_c; see Fig. S6). Data shown are representative examples measured on single networks. Symbols are shown for clarification only, and every fifth data point is shown. (*A*) The measurements for 4 mg/mL collagen networks polymerized at temperatures between 26 and 37°C are given (see legend). (*B*) Simulation data for 2D fibrous networks with a fixed dimensionless rigidity, $\tilde{\kappa} = 10^{-4}$, and varying average connectivity $\langle z \rangle$ are given (see legend). To see this figure in color, go online.

A closer inspection of the strain-stiffening curves reveals two distinct stiffening regimes demarcated by two distinct characteristic strain values. The first characteristic strain, which we denote as γ_0, corresponds to the end of the linear elastic regime and onset for strain stiffening (*red symbols* in Fig. 3 *A*). Although γ_0 is difficult to identify unambiguously from the strain-stiffening curves, it can be clearly identified when we plot $K'(\sigma)/\sigma$ as a function of σ (Fig. S5). The second characteristic strain, which we denote as γ_c (*blue symbols* in Fig. 3 *A*), is closer to the failure point. This characteristic strain is well-defined as the inflection point of the strain-stiffening curves (see Fig. S6). We see that both γ_0 and γ_c increase with the polymerization temperature (Fig. 4 *A*).

Can we quantitatively explain these changes in the strain dependent elasticity of the collagen networks in terms of their architecture? To answer this, we employ a computational model that represents a collagen network as a disordered network of elastic fibers, based on an initial 2D triangular lattice (20,25,40). We use 2D simulations because these are much less computationally intensive than 3D simulations, which allows us to scan a wider parameter space with larger systems that are less sensitive to finite-size effects. Prior work has shown good consistency between 2D and 3D simulations of such models, provided that the average coordination number $\langle z \rangle$ is well below the 2D isostatic point of four (28,45). This model assumes that thermal fluctuations are negligible, an assumption that is amply justified by fluctuation analysis (46) and various mechanical measurements (47–53) on single collagen fibers. Each filament is assigned a stretching modulus, μ_s, and a bending modulus, κ. These two parameters define a dimensionless measure of the relative bend-stretch stiffness: $\tilde{\kappa} = \kappa/\mu_s l_c^2$. We note that our model networks are disordered even though they are based on an initial lattice structure: both the connectivity and fiber length, for instance, vary from point to point within the network.

Consistent with the experimental observations, the simulations reveal a two-stage strain-stiffening response with an onset strain γ_0 (*red circles*) and an inflection at a critical strain γ_c (*blue squares*), as shown in Fig. 3 *B* (see also Figs. S5 and S6). As we progressively increase $\langle z \rangle$ from 3.12 (*black line*) to 3.56 (*lightest gray line*), we see that G_0 increases, whereas γ_0 and γ_c decrease. These shifts are qualitatively consistent with the shifts we observe in

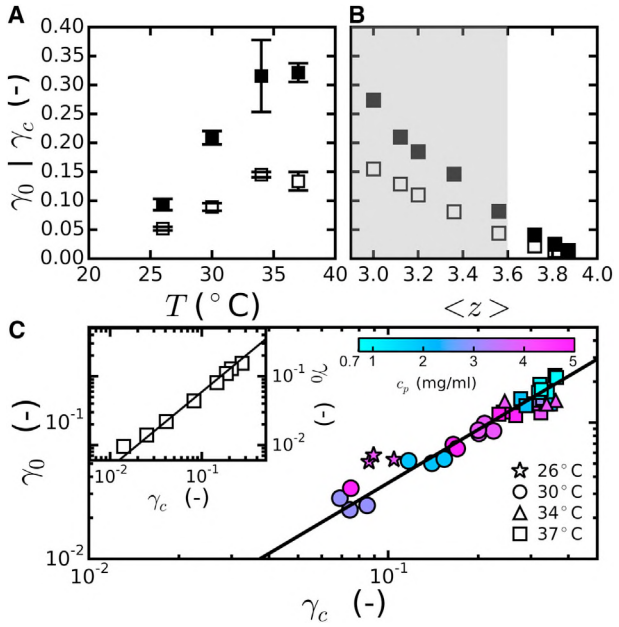

FIGURE 4 Comparison of the onset strain and the critical strain that characterize the strain-stiffening response of collagen networks with predictions for 2D fibrous networks. (*A*) Measurements of γ_0 (*open symbols*) and γ_c (*closed symbols*) for 4 mg/mL collagen networks are given. Data points are averages ± SD for three samples per condition. (*B*) Corresponding simulation results are given showing the $\langle z \rangle$ -dependence of γ_0 and γ_c for 2D networks with $\tilde{\kappa} = 10^{-4}$, a value that is representative of collagen networks at concentrations in the range of several mg/mL (25). The $\langle z \rangle$ -range relevant to the experiments is highlighted in gray. (*C*) The experiments (main plot) are in excellent agreement with the simulations (*inset*), which predict a power-law dependence of γ_0 on γ_c with an exponent given by $\phi - f$. The lines have slopes of 1.3 (main) and 1.1 (*inset*), based on predicted values of ϕ and f in Table S2. Data points represent individual measurements (at least three per condition) obtained at collagen concentrations c_p between 0.7 and 5 mg/mL and polymerization temperatures between 26 and 37°C (see legends). To see this figure in color, go online.

collagen networks as we reduce the polymerization temperature. We therefore hypothesize that the temperature dependence of the nonlinear elasticity of collagen networks may be caused by a change in the network connectivity.

To test this hypothesis, we directly compare the γ_0 and γ_c values determined in experiments and in simulations (Fig. 4, *A* and *B*). In the experimentally relevant $\langle z \rangle$ range (between 3 and 3.5), the strain values in experiments and simulations are in close agreement. Using the simulations as a reference point, we can infer from the correspondence with the experiments that the shift to larger γ_0 values as the polymerization temperature is raised from 26 to 37°C is consistent with a decrease in $\langle z \rangle$ from ~3.5 to 3 (see Fig. 5 *B*; Table S1). We note that all concentrations tested at 30°C show higher $\langle z \rangle$ values compared to the 37°C case (Fig. 5 *A*). At 37°C, $\langle z \rangle$ is below three at the lowest concentrations of 0.7 and 1 mg/mL, whereas it is close to three for collagen concentrations between 2 and 4 mg/mL and increases to almost 3.2 at 5 mg/mL (see Fig. 5 *A* (*black squares*); Table S1).

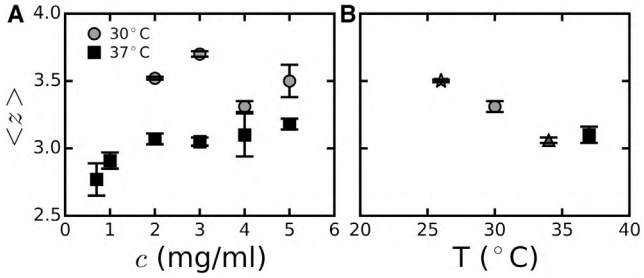

FIGURE 5 Average connectivity $\langle z \rangle$ of collagen networks inferred from rheology data by calibrating measurements of γ_0 with simulation data for 2D fibrous networks (see Fig. 4, *A* and *B*). (*A*) The concentration dependence of $\langle z \rangle$ at a polymerization temperature of 37°C (*black squares*) and 30°C (*gray circles*) is given. (*B*) The temperature dependence of $\langle z \rangle$ at a collagen concentration of 4 mg/mL is shown. Data points are averages ± SD for three samples per condition. The data are also tabulated in Table S1.

The values of $\langle z \rangle$ we infer from the nonlinear rheology predicted by our model are qualitatively consistent with the SEM images of 4 mg/mL networks prepared at different temperatures. In these images, we observe predominantly threefold branches and fourfold junctions (see Fig. S7). The images do not reveal a significant dependence of $\langle z \rangle$ on polymerization temperature. It is difficult, however, to measure $\langle z \rangle$ reliably from imaging alone. The problem is that imaging cannot unambiguously distinguish whether an apparent junction of two fibers in a static image is a cross-linked pair or just an entangled pair, and it is furthermore difficult to determine whether the fiber ends are cross-linked to other fibers or dangling. The SEM images show that fibers emerging from branch points often have unequal diameters. In the context of our model, such variation in fiber diameter and possible unequal distribution of material at branch ($z = 3$) or crossing ($z = 4$) points represents a kind of (quenched) disorder. We do not include variation in the fiber diameter in this model. In previous theoretical work in which we tested the effect of inhomogeneous fiber diameter in branched networks, we did not find qualitative differences in the network rheology (54).

As a further test of our hypothesis that the fibrous network model can explain the nonlinear elasticity of collagen networks, we check for the correlation between γ_0 and γ_c. The simulations predict that γ_0 should increase with γ_c according to $\gamma_0 \sim \gamma_c^{(\phi - f)}$ (*inset* of Fig. 4 *C*). The physical basis of this relationship is that collagen networks undergo a strain-controlled transition from an elastic regime governed by fiber bending to an elastic regime governed by fiber stretching when the strain reaches γ_c (25,40). Simulations predict that this phase transition is governed by two critical exponents, ϕ and f, which are nearly identical for 2D and 3D networks (25,29). Using values for these exponents determined in simulations of 2D lattices for varying $\langle z \rangle$ (see Table S2), we find quantitative agreement of the measured values of γ_0 and γ_c with the theory (*solid line*) for all polymerization temperatures (*color-coded symbols*) without any

adjustable parameters (Fig. 4 *C*). This remarkable agreement provides additional strong evidence that collagen networks over a range of concentrations (0.7–5 mg/mL) and polymerization temperatures (26–37°C) can be modeled as athermal random networks of elastic fibers. Our findings furthermore suggest that the nonlinear elasticity of collagen networks is sensitive to small changes in average network connectivity that are not readily apparent from microscopy images.

Low-strain mechanics of collagen

We have shown that a coarse-grained model that describes collagen networks as disordered networks of elastic fibers can successfully explain the nonlinear elastic response of collagen networks over a wide range of collagen concentrations and polymerization temperatures. An additional critical test of the model is whether it can also predict the magnitude of the linear elastic modulus at small strains below the onset of the nonlinear regime. We find that the linear modulus of the collagen networks, as quantified by $G_0 = G'$ (0.5 Hz), shows a nonmonotonic dependence on polymerization temperature (*solid symbols* in Fig. 6 *A*): at a concentration of 4 mg/mL, the collagen gels are stiffest at 22 and 26°C, whereas they are softest between 30 and 37°C. To test whether we can relate this temperature dependence to the changes in network structure, we compare the measured moduli to theoretical predictions, according to which G_0 can be written as follows:

$$G_0 = F(z)E\varphi^2, \tag{1}$$

where $F(z) \simeq (A/z)(\sqrt{2}/12\pi)(L/l_c)^2$ and L is the average fiber length. The network geometry as characterized by $\langle z \rangle$ enters Eq. 1 only through $F(z)$. In case $\langle z \rangle$ (and therefore $F(z)$) is independent of collagen concentration, the linear modulus should scale quadratically with the fiber-volume fraction φ, consistent with prior athermal network models (30,31). Any deviation from a quadratic scaling therefore signifies a concentration dependence of $\langle z \rangle$. We observe a clear deviation from this scaling for collagen networks polymerized at 37°C, where the power-law exponent is 2.6 (indicated by the *line* in Fig. 6 *B*). This indicates an increase of $\langle z \rangle$ with concentration, consistent with the conclusions we draw from the concentration dependence of γ_0 (see Fig. 5 *A*). For networks polymerized at 30°C, the concentration dependence is closer to quadratic, with a best-fit exponent of 2.1.

To test this apparent self-consistent agreement between the linear and nonlinear elastic behavior more closely, we compare for each experimental condition the measured G_0 with the theoretically expected modulus, calculated from Eq. 1 using as input the $\langle z \rangle$ values inferred from the onset strain (see Table S1). The sole unknown parameter used for fitting is the fiber Young's modulus E. As shown in Fig. 6, the theory captures both the temperature dependence of G_0 at a fixed collagen concentration (Fig. 6 *A*) and the concentration dependence of G_0 at 37°C (Fig. 6 *B*) and 30°C (Fig. 6 *C*) rather well when we assume $E = 1.1$ MPa throughout. Note that we excluded data obtained for networks polymerized at 22°C from this analysis, because these networks were too heterogeneous to extract reliable values for the fiber mass-length ratio by light scattering (see Fig. S2 *A*), and also because the nonlinear rheology data show hysteresis (Fig. S4 *A*).

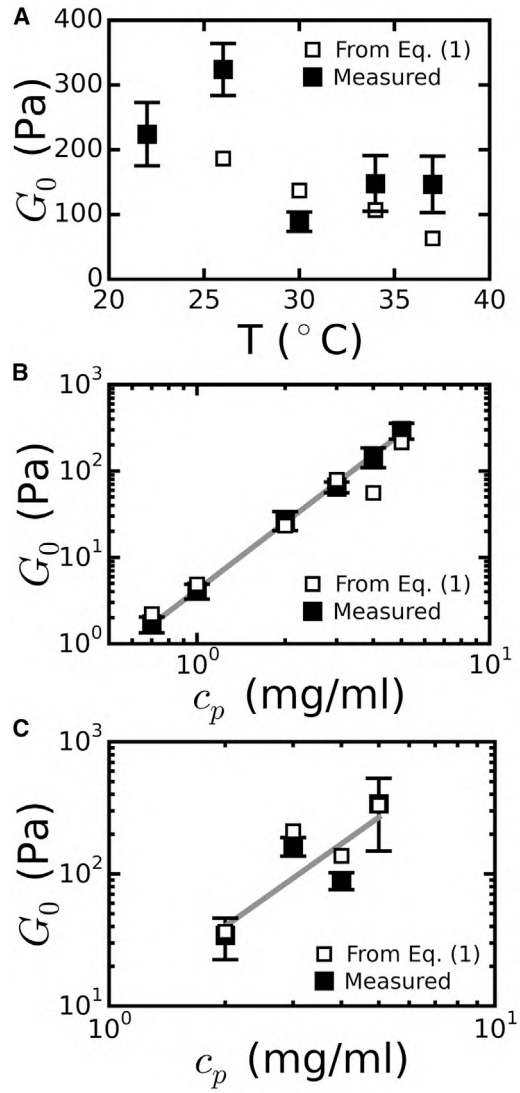

FIGURE 6 Comparison between measurements of the linear elastic modulus of collagen gels (*closed symbols*) and theoretical predictions for 3D fibrous networks (*open symbols*). The theoretical values are calculated according to Eq. 1, which takes as input $\langle z \rangle$ as inferred from the nonlinear rheology (Fig. 5; Table S1), the fiber mass length as measured by turbidimetry (Fig. 2), and the fiber Young's modulus E as the sole fitting parameter. (*A*) The temperature dependence of $G_0 = G'$ (0.5 Hz) for 4 mg/mL collagen gels is shown. (*B*) The concentration dependence of G_0 for networks polymerized at 37°C and (*C*) 30°C is shown. The lines in (*B*) and (*C*) denote power-law fits with exponents of 2.6 and 2.1, respectively. Data points are averages ± SD for three samples per condition. The data are also tabulated in Table S1.

The agreement between theory and experiment is less good in Fig. 6 *A* than it is in Fig. 6, *B* and *C*. We suspect that this is due to inaccuracies in the fiber mass-length ratio μ, which is required as input to calculate G_0 (see Eq. S8). We obtain μ from turbidimetry, which requires a theoretical model with several simplifying assumptions, including diameter monodispersity. We suspect that μ is more accurate for the more homogeneous networks formed at 30 and 37°C (data in Fig. 6, *B* and *C*) than for the somewhat bundled networks formed at lower temperatures (data in Fig. 6 *A*). Note that the fact that we use experimental input for μ, and that μ apparently changes with polymerization temperature and collagen concentration, also explains the nonmonotonicity of the predicted dependencies of G_0 in Fig. 6. Altogether, we think that the overall good agreement of theory and experiment over a range of collagen concentrations and assembly temperatures and for a reasonable value of E (see Discussion) provides convincing evidence that collagen networks over a wide range of assembly conditions can indeed be modeled as random networks of elastic fibers.

Stress-stiffening behavior of collagen networks

In addition to considering the dependence of collagen elasticity on strain, it is also instructive to consider its dependence on the applied shear stress. As shown in Fig. 7 *A*, K' increases as a power law in σ with a stiffening exponent β that increases as the polymerization temperature is raised. As shown in Fig. 7 *C*, β increases from a value close to one at 26°C to 1.6 at 37°C. When we perform a set of simulations on 2D fibrous networks for connectivities $\langle z \rangle$ between 3.12 and 3.56 and a fixed $\tilde{\kappa}$ of 10^{-4}, we find that β strongly depends on $\langle z \rangle$ (Fig. 7 *B*). By contrast, β changes little when $\tilde{\kappa}$ is varied in the relevant $\langle z \rangle$ range (Fig. S8 *B*). Consistent with this prediction, we find only a weak concentration dependence for β in the experiments (Fig. S8 *A*).

As summarized in Fig. 7 *D*, the simulations predict that β should decrease with increasing $\langle z \rangle$. The predicted values for $\beta \sim 1.0$–1.6 in the relevant $\langle z \rangle$ range between 3 and 3.5 are consistent with the experimentally observed range of β-values. By comparing the observed temperature dependence and predicted $\langle z \rangle$ -dependence of β, we infer an apparent decrease of $\langle z \rangle$ from 3.7 to 3 as we raise the polymerization temperature from 26 to 37°C. This conclusion is entirely in line with the apparent decrease of $\langle z \rangle$ we inferred from the temperature dependence of γ_0 and γ_c. We once again conclude that the nonlinear elasticity of collagen networks appears to be sensitive to small changes in network connectivity.

Normal stress stabilizes collagen networks

We have shown that both the linear and nonlinear elasticity of collagen networks are in close agreement with theoretical predictions for networks of elastic fibers. As a final critical test of the model, we consider the normal stress that the networks develop when they are sheared. It is well established that fibrous networks develop a negative (contractile) normal stress when they are sheared between two plates with a fixed gap (37). Several analytical models and simulations for fibrous networks predict that stress-stiffening should be accompanied by an increase of the magnitude of this normal stress (37,55,56). Recent simulations suggest that there is a fundamental connection between the elastic modulus K' and the self-generated normal stress σ_N in submarginal fibrous networks under shear (20,40). Specifically, it was shown that K' grows in direct proportion to σ_N:

$$K' \simeq G_0 + \chi|\sigma_N|, \tag{2}$$

where χ is the susceptibility. It was hypothesized that the normal stress stabilizes the network once the network is strained out of the linear regime ($\gamma > \gamma_0$) and before it undergoes a strain-driven transition to a stretch-dominated regime (at γ_c). Here, we experimentally test this intriguing hypothesis by measuring the normal stress that collagen gels exert on the top plate of the rheometer as a function of the applied shear stress. As shown in Fig. 8 *A*, shearing indeed induces a significant negative normal stress that increases in magnitude with increasing shear stress. We observe this effect for all collagen gels polymerized at concentrations

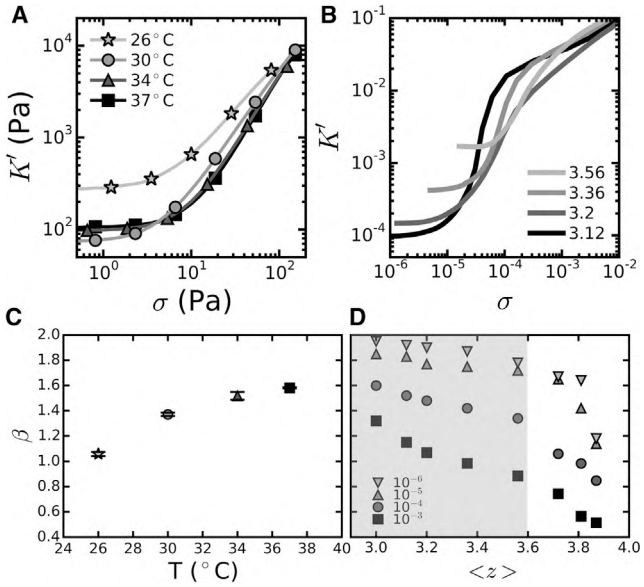

FIGUR E 7 Comparison of the stress-stiffening response of collagen networks with predictions for 2D fibrous networks. (*A*) Example stiffening curves for 4 mg/mL collagen gels polymerized at different temperatures are given (see legend). The data shown are representative measurements on single networks. (*B*) Example stiffening curves for 2D fibrous networks with different connectivities $\langle z \rangle$ (see legend) and $\tilde{\kappa} = 10^{-4}$ (*B*) are given. (*C*) The stiffening exponent β, defined as the maximal slope of the stress-stiffening curves in the nonlinear regime, increases with temperature. Data points are averages ± SD for three samples per condition. (*D*) The simulations show that β depends on both $\tilde{\kappa}$ and $\langle z \rangle$. The highlighted region depicts the $\langle z \rangle$ -range relevant to the experiments.

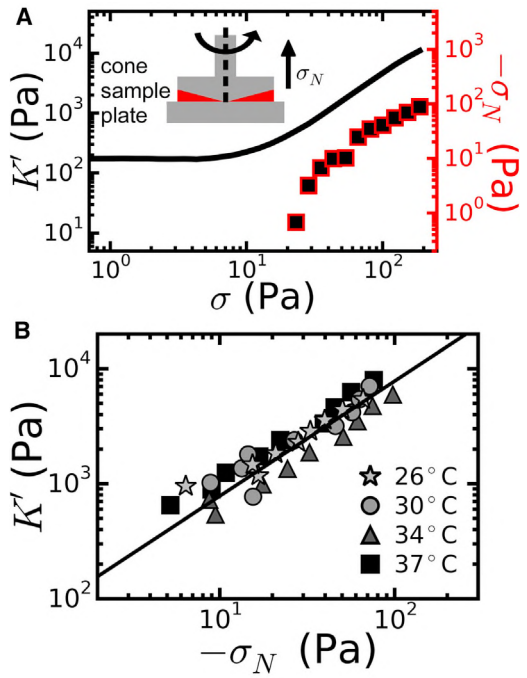

FIGURE 8 Sheared collagen networks develop a negative normal stress whose magnitude is linearly related to the nonlinear elastic modulus. (*A*) An example measurement is given, showing simultaneous stiffening (*black line*, *left y axis*) and the development of a negative normal stress (σ_N, *right y axis*) for a 4 mg/mL collagen network at 37°C. The inset shows a schematic side view of the cone-plate measurement geometry and indicates the directions of the shear stress σ and normal stress σ_N. (*B*) K increases linearly with $-\sigma_N$ for 4 mg/mL collagen gels polymerized at temperatures between 26 and 37°C (see legend). One representative measurement per temperature condition is plotted. The solid line shows the expected linear dependence from Eq. 2. To see this figure in color, go online.

above ~1 mg/mL and polymerization temperatures of 26°C or higher. We were unable to obtain measurable normal-stress signals for collagen gels polymerized at 22°C, likely because we are unable to reach large enough strains to enter far enough into the nonlinear regime. We note that we always observed a nonzero normal stress even at small strain, which is likely dominated by the surface tension of the sample at its edge (38). Because this effect is not related to the elastic properties of the collagen network itself, we subtracted this offset from the normal stress data.

To test the validity of the model, we first verified that K' exhibits the expected linear dependence on σ_N by plotting data for different collagen concentrations and polymerization temperatures together. As shown in Fig. 8 *B*, we indeed find a linear dependence of K' on σ_N. According to Eq. 2, we should in principle be able to determine the susceptibility χ from a linear fit to these data. However, because σ_N was rather noisy, especially at collagen concentrations below 2 mg/mL, we used an alternative approach. According to the simulations, right at the point at which strain-stiffening sets in, the shear stress and the normal stress are comparable in magnitude (37,40,55). We can therefore rewrite Eq. 2 as $K'/\sigma_0 \simeq \chi$. Using the σ_0 -values we already determined from stress-stiffening curves, we find that χ is linear in $1/\gamma_0$ (see Fig. 9 *A*), in line with the simulations (*inset*). Finally, taking these values for χ as input, we tested whether the stress-stiffening behavior of collagen networks is controlled by normal stress as predicted by Eq. 2. As shown in Fig. 9 *B*, we indeed observe a reasonable correspondence between the stiffening behavior predicted on the basis of the measured normal stress response (*lines*) and the measured stiffening response (*symbols*) for 4 mg/mL collagen networks polymerized at temperatures of 26°C and above. We observe a similarly good agreement at other collagen concentrations (Fig. S9). We consistently observe a factor of two difference between

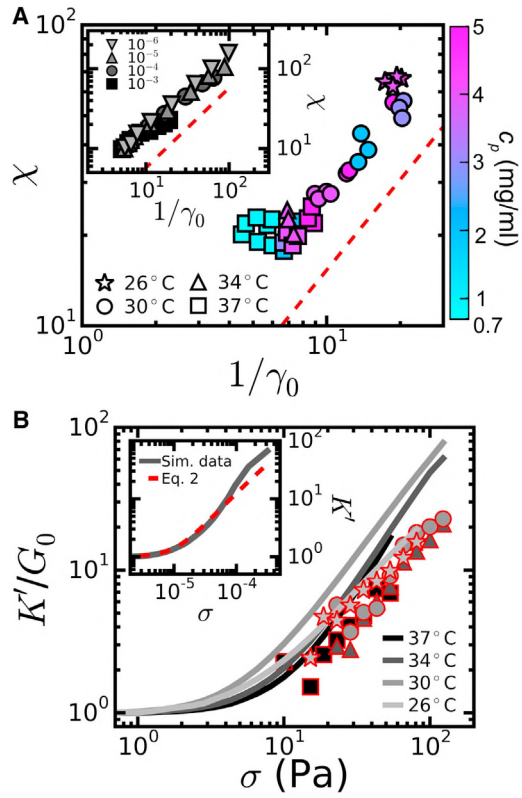

FIGURE 9 The self-generated normal stress stabilizes collagen networks and controls the initial strain-stiffening response. (*A*) Both in experiments (main plot) and in simulations (*inset*), the susceptibility χ determined from stress-stiffening curves (*symbols*) is linear in $1/\gamma_0$ (*dashed lines*). Collagen gels were polymerized at temperatures between 26 and 37°C and collagen concentrations between 0.7 and 5 mg/mL (*blue-pink*) (see legend and *color bar* on the right). Simulations in the inset were performed for different $\tilde{\kappa}$ values (see legend) and for $\langle z \rangle$ between 3 and 3.87 (see Table S2). (*B*) The stress-stiffening response of 4 mg/mL collagen networks polymerized at temperatures ranging from 26 to 37°C is correctly predicted by Eq. 2 (*red symbols*, calculated using measurements of the normal stress as input) to within a factor of two. (*B*, *inset*) The simulations likewise show agreement between simulated K' values (*gray line*) and calculations from the normal stress using Eq. 2 (*red dashed line*), as exemplified for a network with $\tilde{\kappa} = 10^{-4}$ and $\langle z \rangle = 3.2$. In (*A*), all individual measurements (at least three per conditions) are plotted, whereas in (*B*), representative curves are shown. To see this figure in color, go online.

theory and experiment, perhaps because Eq. 2 is only valid at stresses below σ_c. Altogether, the experiments provide strong support for the hypothesis, made on the basis of simulations, that a shear-induced normal force governs the nonlinear elasticity of collagen gels at intermediate strains between γ_0 and γ_c. Moreover, this agreement provides further evidence that elastic fiber network models provide an appropriate description of collagen elasticity over a wide range of assembly conditions.

DISCUSSION

We combined experiments and computational modeling to elucidate the origin of the nonlinear elastic properties of fibrillar collagen networks. By varying the polymerization temperature between 22 and 37°C and the collagen monomer concentration between 0.5 and 5 mg/mL, we obtained collagen networks with an architecture ranging from a sparse meshwork of thick collagen fibril bundles to a dense meshwork of thin collagen fibrils. We modeled the networks as random networks of stiff fibers with an average local connectivity between three (branch points) and four (junctions of crosslinked fibers). We showed that the model provides a self-consistent description of all aspects of the nonlinear elastic response of collagen networks (i.e., G_0, γ_0, γ_c, β, and the relation between shear modulus and normal stress) with reasonable parameter values for the average connectivity $\langle z \rangle$ and the fiber Young's modulus E. We furthermore showed that the quantitative agreement between theory and experiment holds over the entire concentration range and all polymerization temperatures between 26 and 37°C. Only for networks formed at 22°C could we not use the model, because these networks were too heterogeneous and exhibited marked inelastic behavior. Several recent studies likewise identified inelastic behavior in collagen networks (57,58), which allows cells to align and bundle collagen fibers by applying traction forces (59–61). Our data suggest that the extent to which collagen behaves inelastically can be tuned by the polymerization temperature, probably through a modulation of the hydrophobic interactions that dominate collagen association. It will be an interesting challenge to include such inelastic effects in our random network model by extending it with transient fiber-fiber bonding.

Our work suggests that microscopic properties of collagen can be inferred from macroscopic rheology data by comparing experiments against theoretical predictions for fibrous networks. The conditions under which this approach is valid are well defined and easily verified by microscopy and rheology experiments: the network needs to be isotropic, athermal, elastic, and subisostatic (i.e., $\langle z \rangle$ needs to be below six).

We propose that the bending rigidity of the fibrils can be inferred from the linear elastic modulus, G_0. We were able to explain the dependence of G_0 on collagen concentration and polymerization temperature with a single value for the fibril Young's modulus of 1.1 MPa. It is difficult to directly validate this number, because this requires challenging in situ micromanipulation measurements on individual collagen fibrils within 3D networks. Until now, micromanipulation measurements have been restricted to isolated collagen fibrils. Furthermore, those measurements vary over a wide range depending on whether the fibers are reconstituted from purified collagen or extracted from tissue, on sample preparation, and on the measurement technique. A direct comparison to literature values is therefore difficult. Values for (hydrated) native collagen fibrils range from 2–5 MPa (51) to 10–30 MPa (53), 50–120 MPa (48,49,52), and even 100–360 MPa (47). The few reports we are aware of in which reconstituted collagen fibrils were used report smaller moduli of just a few kPa (62) or several MPa (53). It is not surprising that reconstituted fibrils would be softer than native fibrils, given that they are much less cross-linked (63,64). In light of the existing literature, we consider the value of 1.1 MPa we infer for the Young's modulus of reconstituted collagen I fibers as reasonable. In the future, it will be interesting to perform micromanipulation measurements on fibrils within 3D networks using optical or magnetic tweezers to test the Young's modulus under physiologically relevant assembly conditions.

Our findings also suggest that the nonlinear elastic response of collagen networks can reveal microscopic properties of the networks, specifically the average coordination number $\langle z \rangle$. The strain-stiffening response has two phases, with an onset of stiffening at a strain γ_0 and a strain-controlled transition from a bend-dominated regime to a stretch-dominated elastic regime at a strain γ_c. We observed that γ_0 and γ_c both increase with increasing polymerization temperature. In the context of the model, this observation tells us that $\langle z \rangle$ decreases from 3.5 to 3 on going from 26 to 37°C. We reach the same conclusion when we consider the linear modulus G_0, which drops on going from 26 to 30°C, and the stress-stiffening exponent, β, which increases with increasing polymerization temperature. The structure of collagen networks is known to be kinetically determined. With increasing temperature, we expect an increased rate of nucleation and growth of collagen fibers, which will increase the likelihood of branching. Networks formed at 37°C have $\langle z \rangle$ close to 3, consistent with a highly branched network, over a range of concentrations between 2 and 5 mg/mL. Indeed, with increasing temperatures, we expect an increased rate of nucleation and growth of collagen fibers, which will increase the likelihood of branching. Below 2 mg/mL, we find $\langle z \rangle$ values below 3, suggesting the presence of dangling (elastically inactive) ends. Admittedly, the determination of $\langle z \rangle$ is currently model dependent. We find that it is difficult to determine $\langle z \rangle$ precisely from imaging alone. Imaging cannot distinguish whether fibers form a true junction or are merely entangled or in close proximity. Moreover, it is difficult to determine whether the fiber ends

are cross-linked to other fibers or dangling. A further issue is the difficulty in reliably tracing all fibers in dense 3D networks (26,65,66). In the future, it may be possible to solve these issues by using time-lapse imaging or micromanipulation experiments to test whether an apparent junction of two fibers is a cross-linked pair or just an entangled pair. Our work suggests that rheological measurements meanwhile provide a robust and convenient assay to measure the ensemble-averaged network connectivity. At the same time, the sensitivity of the rheology to small changes in connectivity can explain the diversity of concentration dependencies observed in studies performed with different collagen batches and assembly conditions, with power-law dependencies of G_0 on concentration with exponents varying between one and three (18,19,32–36).

Our model provides a mechanistic basis for explaining the strain-stiffening behavior that is characteristic of collagen networks and collagenous tissues. Earlier computational studies had suggested that strain-stiffening originates from a transition from bending-dominated elasticity at low strain to a stretch-dominated elasticity regime at high strain (67). However, here we showed that collagen networks already stiffen substantially, well before the transition to the stretch-dominated state occurs. Thus, the initial strain-stiffening response that sets in at γ_0 is actually not caused by a bend-to-stretch transition. A recent theoretical study put forward the hypothesis based on simulation data that the initial stiffening is induced by a self-generated normal stress (20,40). Here, we experimentally confirm this hypothesis. We find that sheared collagen networks indeed develop a large negative (contractile) normal stress and that the elastic modulus K' grows in direct proportion to the magnitude of this normal stress. It is only for strains above γ_c that the networks undergo a transition to a rigid stretch-dominated elastic regime (25,29).

The microscopic model we propose opens up several interesting avenues of future research. First, our findings provide a starting point to develop multiscale models of collagen networks that incorporate the different hierarchical levels of structure. In this study, we coarse-grained the collagen fibers as uniform elastic beams. This approach allows us to model the effective elastic properties of the fibers, but it cannot account for the mechanical anisotropy of collagen fibers associated with their bundle-like structure (68,69) nor for strain-dependent changes in their molecular packing (9,70). Depending on the required level of detail, the fibers could be modeled as Timoshenko beams to account for intrafibrillar shear (69), or one could even integrate the model with constitutive relations determined from full-atom simulations to account for the viscoelastic properties of the fibers (22) and strain-induced fiber lengthening via subunit sliding (20).

Second, our findings provide a quantitative framework to understand how auxiliary extracellular matrix proteins regulate the structure and mechanics of collagen networks. Although collagen I is the most abundant type of collagen in noncartilaginous tissues (>90%), it nevertheless always forms "heterotypic" fibrils together with other fibrillar collagens such as collagens III and V and noncollagenous molecules such as glycosaminoglycans. This co-assembly is thought to provide an essential mechanism for regulating the diameter of the fibrils and tailoring collagen networks for the specific biomechanical requirements of different adult tissues and of remodeling tissues (1). Using the random network model, it should now be possible to relate the mechanical properties of collagen networks to the underlying changes in structure at both the fibril and network scale.

Third, our findings provide a quantitative framework to investigate the mechanobiology of cell-matrix interactions. Cell-seeded collagen networks are widely used as extracellular matrix model systems for tissue morphogenesis, wound healing, cell migration, and cancer biology (10,11). The elastic modulus of collagen networks was shown to influence many cell functions such as cell migration and proliferation (17,71,72). Our work facilitates systematic studies of this mechanoregulation by making it possible to design the network structure to achieve a desired elastic response. Our work also facilitates measurements of the transmission of forces generated by cells cultured in collagen networks. Recently, several methods have been proposed to infer the traction forces that cells exert on the collagen matrix at focal adhesion sites from imaging-based measurements of the matrix strain (61,73,74). This has been a challenging problem due to the fibrous architecture of collagen networks, which causes cells to stiffen the matrix around them (75,76) and makes force transmission long-ranged (61,77). Our findings strongly support the validity of using athermal random network models to provide a quantitative relation between stresses and strains in collagen matrices.

CONCLUSIONS

Our findings show that models of disordered networks of elastic fibers provide a unifying framework to understand the relation between collagen network mechanics and microstructure over a wide range of assembly conditions as long as the network structure is isotropic and sufficiently uniform. Interestingly, our work suggests that macroscopic measurements of the nonlinear elastic behavior are able to reveal microscopic information about the average network connectivity, a parameter that is difficult to determine reliably from microscopy images. It will be important in future work to find model-independent methods of measuring the network connectivity to validate this conclusion based on imaging. Our work establishes a strong basis to predict the elastic properties of more physiologically relevant collagen systems, in which the fibril diameter is regulated by copolymerization of collagen I with other fibril-forming collagens and glycosaminoglycans. Moreover, our study provides a

quantitative framework to design collagen networks with desired mechanical properties, which is useful for biophysical studies on the mechanoregulation of cell migration, wound healing, and tissue morphogenesis. Our model is generally applicable to fibrous networks, provided that the networks are isotropic, athermal, and subisostatic. There are many biological materials that fulfill these criteria in addition to collagen, including fibrin, which mediates blood clotting in animals, and cellulose, which provides support to plant and tree tissues.

SUPPORTING MATERIAL

Supporting Materials and Methods, eleven figures, and two tables are available at http://www.biophysj.org/biophysj/supplemental/S0006-3495(18)30538-1.

AUTHORS CONTRIBUTIONS

K.A.J., A.J.L., A.S., G.H.K., and F.C.M. designed research. K.A.J., A.J.L., A.S., and R.R. performed research and analyzed data. All authors wrote the manuscript.

ACKNOWLEDGMENTS

The authors thank B. Vos for analyzing and discussing the turbidity data and F. Burla for critically reading the manuscript.

F.C.M. was supported in part by the National Science Foundation (grant PHY-1427654). This work was further supported by the Foundation for Fundamental Research on Matter, which is part of the Netherlands Organisation for Scientific Research, and by NanoNextNL, a micro- and nanotechnology program of the Dutch Government and 130 partners.

SUPPORTING CITATIONS

References (78–87) appear in the Supporting Material.

REFERENCES

1. P. Fratzl, ed 2008. Collagen Structure and Mechanics Springer Science+Business Media, Berlin, Germany.
2. Kjaer, M., H. Langberg, …, S. P. Magnusson. 2009. From mechanical loading to collagen synthesis, structural changes and function in human tendon. *Scand. J. Med. Sci. Sports.* 19:500–510.
3. Boote, C., C. S. Kamma-Lorger, …, K. M. Meek. 2011. Quantification of collagen organization in the peripheral human cornea at micron-scale resolution. *Biophys. J.* 101:33–42.
4. Mouw, J. K., G. Ou, and V. M. Weaver. 2014. Extracellular matrix assembly: a multiscale deconstruction. *Nat. Rev. Mol. Cell Biol.* 15:771–785.
5. Kai, F., H. Laklai, and V. M. Weaver. 2016. force matters: biomechanical regulation of cell invasion and migration in disease. *Trends Cell Biol.* 26:486–497.
6. Fung, Y. 1984. Structure and stress-strain relationship of soft tissues. *Am. Zool.* 24:13–22.
7. Shadwick, R. E. 1999. Mechanical design in arteries. *J. Exp. Biol.* 202:3305–3313.
8. Orgel, J. P., T. C. Irving, …, T. J. Wess. 2006. Microfibrillar structure of type I collagen *in situ*. *Proc. Natl. Acad. Sci. USA.* 103:9001–9005.
9. Misof, K., G. Rapp, and P. Fratzl. 1997. A new molecular model for collagen elasticity based on synchrotron X-ray scattering evidence. *Biophys. J.* 72:1376–1381.
10. Grinnell, F., and W. M. Petroll. 2010. Cell motility and mechanics in three-dimensional collagen matrices. *Annu. Rev. Cell Dev. Biol.* 26:335–361.
11. Brown, R. A. 2013. In the beginning there were soft collagen-cell gels: towards better 3D connective tissue models? *Exp. Cell Res.* 319:2460–2469.
12. Roeder, B. A., K. Kokini, …, S. L. Voytik-Harbin. 2002. Tensile mechanical properties of three-dimensional type I collagen extracellular matrices with varied microstructure. *J. Biomech. Eng.* 124:214–222.
13. Raub, C. B., J. Unruh, …, S. C. George. 2008. Image correlation spectroscopy of multiphoton images correlates with collagen mechanical properties. *Biophys. J.* 94:2361–2373.
14. Sapudom, J., S. Rubner, …, T. Pompe. 2015. The phenotype of cancer cell invasion controlled by fibril diameter and pore size of 3D collagen networks. *Biomaterials.* 52:367–375.
15. Raub, C. B., V. Suresh, …, S. C. George. 2007. Noninvasive assessment of collagen gel microstructure and mechanics using multiphoton microscopy. *Biophys. J.* 92:2212–2222.
16. Hwang, Y.-J., and J. G. Lyubovitsky. 2011. Collagen hydrogel characterization: multi-scale and multi-modality approach. *Anal. Methods.* 3:529–536.
17. Wolf, K., M. Te Lindert, …, P. Friedl. 2013. Physical limits of cell migration: control by ECM space and nuclear deformation and tuning by proteolysis and traction force. *J. Cell Biol.* 201:1069–1084.
18. Motte, S., and L. J. Kaufman. 2013. Strain stiffening in collagen I networks. *Biopolymers.* 99:35–46.
19. Vader, D., A. Kabla, …, L. Mahadevan. 2009. Strain-induced alignment in collagen gels. *PLoS One.* 4:e5902.
20. Licup, A. J., S. Münster, …, F. C. MacKintosh. 2015. Stress controls the mechanics of collagen networks. *Proc. Natl. Acad. Sci. USA.* 112:9573–9578.
21. Kurniawan, N. A., L. H. Wong, and R. Rajagopalan. 2012. Early stiffening and softening of collagen: interplay of deformation mechanisms in biopolymer networks. *Biomacromolecules.* 13:691–698.
22. Gautieri, A., S. Vesentini, …, M. J. Buehler. 2011. Hierarchical structure and nanomechanics of collagen microfibrils from the atomistic scale up. *Nano Lett.* 11:757–766.
23. Varma, S., J. P. Orgel, and J. D. Schieber. 2016. Nanomechanics of type I collagen. *Biophys. J.* 111:50–56.
24. Chandran, P. L., and V. H. Barocas. 2006. Affine versus non-affine fibril kinematics in collagen networks: theoretical studies of network behavior. *J. Biomech. Eng.* 128:259–270.
25. Sharma, A., A. Licup, …, F. MacKintosh. 2016. Strain-controlled criticality governs the nonlinear mechanics of fibre networks. *Nat. Phys.* 12:584–587.
26. Lindström, S. B., D. A. Vader, …, D. A. Weitz. 2010. Biopolymer network geometries: characterization, regeneration, and elastic properties. *Phys. Rev. E Stat. Nonlin. Soft Matter Phys.* 82:051905.
27. Maxwell, J. 1864. On the calculation of the equilibrium and stiffness of frames. *Philos. Mag.* 27:294–299.
28. Broedersz, C. P., X. Mao, …, F. C. MacKintosh. 2011. Criticality and isostaticity in fibre networks. *Nat. Phys.* 7:983–988.
29. Sharma, A., A. J. Licup, …, F. C. MacKintosh. 2016. Strain-driven criticality underlies nonlinear mechanics of fibrous networks. *Phys. Rev. E.* 94:042407.
30. Kroy, K., and E. Frey. 1996. Force-extension relation and plateau modulus for wormlike chains. *Phys. Rev. Lett.* 77:306–309.
31. Satcher, R. L., Jr., and C. F. Dewey, Jr. 1996. Theoretical estimates of mechanical properties of the endothelial cell cytoskeleton. *Biophys. J.* 71:109–118.

32. Yang, Y. L., L. M. Leone, and L. J. Kaufman. 2009. Elastic moduli of collagen gels can be predicted from two-dimensional confocal microscopy. *Biophys. J.* 97:2051–2060.

33. Kreger, S. T., B. J. Bell, …, S. L. Voytik-Harbin. 2010. Polymerization and matrix physical properties as important design considerations for soluble collagen formulations. *Biopolymers.* 93:690–707.

34. Piechocka, I. K., A. S. van Oosten, …, G. H. Koenderink. 2011. Rheology of heterotypic collagen networks. *Biomacromolecules.* 12: 2797–2805.

35. Velegol, D., and F. Lanni. 2001. Cell traction forces on soft biomaterials. I. Microrheology of type I collagen gels. *Biophys. J.* 81:1786–1792.

36. Miron-Mendoza, M., J. Seemann, and F. Grinnell. 2010. The differential regulation of cell motile activity through matrix stiffness and porosity in three dimensional collagen matrices. *Biomaterials.* 31:6425–6435.

37. Janmey, P. A., M. E. McCormick, …, F. C. MacKintosh. 2007. Negative normal stress in semiflexible biopolymer gels. *Nat. Mater.* 6:48–51.

38. de Cagny, H. C., B. E. Vos, …, D. Bonn. 2016. Porosity governs normal stresses in polymer gels. *Phys. Rev. Lett.* 117:217802.

39. Poynting, J. H. 1909. On pressure perpendicular to the shear planes in finite pure shears, and on the lengthening of loaded wires when twisted. *Proc. Royal Soc. Math. Phys. Eng. Sci.* 82:546–559.

40. Licup, A. J., A. Sharma, and F. C. MacKintosh. 2016. Elastic regimes of subisostatic athermal fiber networks. *Phys. Rev. E.* 93:012407.

41. Forgacs, G., S. A. Newman, …, E. Sackmann. 2003. Assembly of collagen matrices as a phase transition revealed by structural and rheologic studies. *Biophys. J.* 84:1272–1280.

42. Jones, C. A. R., L. Liang, …, B. Sun. 2014. The spatial-temporal characteristics of type I collagen-based extracellular matrix. *Soft Matter.* 10:8855–8863.

43. Zhu, J., and L. J. Kaufman. 2014. Collagen I self-assembly: revealing the developing structures that generate turbidity. *Biophys. J.* 106:1822–1831.

44. Ferri, F., G. R. Calegari, …, M. Rocco. 2015. Size and density of fibers in fibrin and other filamentous networks from turbidimetry: beyond a revisited Carr-Hermans method, accounting for fractality and porosity. *Macromolecules.* 48:5423–5432.

45. Broedersz, C. P., M. Sheinman, and F. C. Mackintosh. 2012. Filament-length-controlled elasticity in 3D fiber networks. *Phys. Rev. Lett.* 108:078102.

46. Bartsch, T. F., M. D. Kochanczyk, …, E. L. Florin. 2016. Nanoscopic imaging of thick heterogeneous soft-matter structures in aqueous solution. *Nat. Commun.* 7:12729.

47. Dutov, P., O. Antipova, …, J. D. Schieber. 2016. Measurement of elastic modulus of collagen type I single fiber. *PLoS One.* 11:e0145711.

48. Shen, Z. L., H. Kahn, …, S. J. Eppell. 2011. Viscoelastic properties of isolated collagen fibrils. *Biophys. J.* 100:3008–3015.

49. Yang, L., K. O. van der Werf, …, M. L. Bennink. 2012. Micromechanical analysis of native and cross-linked collagen type I fibrils supports the existence of microfibrils. *J. Mech. Behav. Biomed. Mater.* 6:148–158.

50. Liu, Y., R. Ballarini, and S. J. Eppell. 2016. Tension tests on mammalian collagen fibrils. *Interface Focus.* 6:20150080.

51. Grant, C. A., D. J. Brockwell, …, N. H. Thomson. 2009. Tuning the elastic modulus of hydrated collagen fibrils. *Biophys. J.* 97:2985–2992.

52. Aifantis, K. E., S. Shrivastava, and G. M. Odegard. 2011. Transverse mechanical properties of collagen fibers from nanoindentation. *J. Mater. Sci. Mater. Med.* 22:1375–1381.

53. Baldwin, S. J., A. S. Quigley, …, L. Kreplak. 2014. Nanomechanical mapping of hydrated rat tail tendon collagen I fibrils. *Biophys. J.* 107:1794–1801.

54. Rens, R., M. Vahabi, …, A. Sharma. 2016. Nonlinear mechanics of athermal branched biopolymer networks. *J. Phys. Chem. B.* 120: 5831–5841.

55. Conti, E., and F. C. Mackintosh. 2009. Cross-linked networks of stiff filaments exhibit negative normal stress. *Phys. Rev. Lett.* 102:088102.

56. Cioroianu, A. R., and C. Storm. 2013. Normal stresses in elastic networks. *Phys. Rev. E Stat. Nonlin. Soft Matter Phys.* 88:052601.

57. Münster, S., L. M. Jawerth, …, D. A. Weitz. 2013. Strain history dependence of the nonlinear stress response of fibrin and collagen networks. *Proc. Natl. Acad. Sci. USA.* 110:12197–12202.

58. Nam, S., K. H. Hu, …, O. Chaudhuri. 2016. Strain-enhanced stress relaxation impacts nonlinear elasticity in collagen gels. *Proc. Natl. Acad. Sci. USA.* 113:5492–5497.

59. Mohammadi, H., P. D. Arora, …, C. A. McCulloch. 2015. Inelastic behaviour of collagen networks in cell-matrix interactions and mechanosensation. *J. R. Soc. Interface.* 12:20141074.

60. Nam, S., J. Lee, …, O. Chaudhuri. 2016. Viscoplasticity enables mechanical remodeling of matrix by cells. *Biophys. J.* 111:2296–2308.

61. Hall, M. S., F. Alisafaei, …, M. Wu. 2016. Fibrous nonlinear elasticity enables positive mechanical feedback between cells and ECMs. *Proc. Natl. Acad. Sci. USA.* 113:14043–14048.

62. Doyle, A. D., N. Carvajal, …, K. M. Yamada. 2015. Local 3D matrix microenvironment regulates cell migration through spatiotemporal dynamics of contractility-dependent adhesions. *Nat. Commun.* 6:8720.

63. Eyre, D., and J. Wu. 2005. Collagen cross-links. *Top. Curr. Chem.* 247:207–229.

64. Gautieri, A., F. S. Passini, …, J. G. Snedeker. 2017. Advanced glycation end-products: Mechanics of aged collagen from molecule to tissue. *Matrix Biol.* 59:95–108.

65. Reese, S. P., N. Farhang, …, J. A. Weiss. 2016. Nanoscale imaging of collagen gels with focused ion beam milling and scanning electron microscopy. *Biophys. J.* 111:1797–1804.

66. Xu, T., D. Vavylonis, …, X. Huang. 2015. SOAX: a software for quantification of 3D biopolymer networks. *Sci. Rep.* 5:9081.

67. Onck, P. R., T. Koeman, …, E. van der Giessen. 2005. Alternative explanation of stiffening in cross-linked semiflexible networks. *Phys. Rev. Lett.* 95:178102.

68. Heim, A. J., T. J. Koob, and W. G. Matthews. 2007. Low strain nanomechanics of collagen fibrils. *Biomacromolecules.* 8:3298–3301.

69. Yang, L., K. O. van der Werf, …, J. Feijen. 2008. Mechanical properties of native and cross-linked type I collagen fibrils. *Biophys. J.* 94:2204–2211.

70. Masic, A., L. Bertinetti, …, P. Fratzl. 2015. Osmotic pressure induced tensile forces in tendon collagen. *Nat. Commun.* 6:5942.

71. Bott, K., Z. Upton, …, S. C. Rizzi. 2010. The effect of matrix characteristics on fibroblast proliferation in 3D gels. *Biomaterials.* 31:8454–8464.

72. Lang, N. R., K. Skodzek, …, B. Fabry. 2015. Biphasic response of cell invasion to matrix stiffness in three-dimensional biopolymer networks. *Acta Biomater.* 13:61–67.

73. Steinwachs, J., C. Metzner, …, B. Fabry. 2016. Three-dimensional force microscopy of cells in biopolymer networks. *Nat. Methods.* 13:171–176.

74. Liang, L., C. Jones, …, Y. Jiao. 2016. Heterogeneous force network in 3D cellularized collagen networks. *Phys. Biol.* 13:066001.

75. Jones, C. A., M. Cibula, …, B. Sun. 2015. Micromechanics of cellularized biopolymer networks. *Proc. Natl. Acad. Sci. USA.* 112:E5117–E5122.

76. van Helvert, S., and P. Friedl. 2016. Strain stiffening of fibrillar collagen during individual and collective cell migration identified by AFM nanoindentation. *ACS Appl. Mater. Interfaces.* 8:21946–21955.

77. Xu, X., and S. A. Safran. 2015. Nonlinearities of biopolymer gels increase the range of force transmission. *Phys. Rev. E Stat. Nonlin. Soft Matter Phys.* 92:032728.

78. Newman, S., M. Cloître, …, D. Beysens. 1997. Viscosity and elasticity during collagen assembly in vitro: relevance to matrix-driven translocation. *Biopolymers.* 41:337–347.

79. Wood, G. C., and M. K. Keech. 1960. The formation of fibrils from collagen solutions. 1. The effect of experimental conditions: kinetic and electron-microscope studies. *Biochem. J.* 75:588–598.

80. Brokaw, J., C. Doillon, …, F. Silver. 1985. Turbidimetric and morphological studies of type I collagen fibre self assembly in vitro and the influence of fibronectin. *Int. J. Biol. Macromol.* 7:135–140.

81. Wess, T. J. 2005. Collagen fibril form and function. *Adv. Protein Chem.* 70:341–374.

82. Baradet, T. C., J. C. Haselgrove, and J. W. Weisel. 1995. Three-dimensional reconstruction of fibrin clot networks from stereoscopic intermediate voltage electron microscope images and analysis of branching. *Biophys. J.* 68:1551–1560.

83. Gersh, K. C., C. Nagaswami, and J. W. Weisel. 2009. Fibrin network structure and clot mechanical properties are altered by incorporation of erythrocytes. *Thromb. Haemost.* 102:1169–1175.

84. de Wild, M., W. Pomp, and G. H. Koenderink. 2013. Thermal memory in self-assembled collagen fibril networks. *Biophys. J.* 105:200–210.

85. L. Landau and E. Lifshiftz, eds 1970. Theory of elasticity, Second Edition Pergamon Press, Oxford.

86. Carr, M. E., Jr., and J. Hermans. 1978. Size and density of fibrin fibers from turbidity. *Macromolecules.* 11:46–50.

87. Yeromonahos, C., B. Polack, and F. Caton. 2010. Nanostructure of the fibrin clot. *Biophys. J.* 99:2018–2027.